

PAPER • OPEN ACCESS

Experimental facility dedicated to detection and prediction of penstock fatigue induced by pressure oscillations

To cite this article: V Hasmatuchi et al 2024 IOP Conf. Ser.: Earth Environ. Sci. 1411 012039

View the article online for updates and enhancements.

You may also like

- Integrity Management of Subsea Pipelines for Water and Gas Transportation in Offshore Gas Storage Facilities
 Jiaxi Fan, Dayong Hao, Min Li et al.
- Preliminary results of the interior features inferred from radargrams, Ulanhada Volcano, Inner Mongolia, China S Dai, Y Su, C Y Ding et al.
- ASO-S orbit evolution and its safety analyses
 Hu Jiang, Cheng Zhu, Lei Deng et al.



Experimental facility dedicated to detection and prediction of penstock fatigue induced by pressure oscillations

V Hasmatuchi¹, R Rittiner¹, S Pires-Boyer¹, C L Lecointre¹, C Nicolet², C Münch-Alligné¹, S Rey-Mermet¹

¹School of Engineering, HES-SO Valais-Wallis, Rue de l'Industrie 23, Sion, Switzerland ²Power Vision Engineering Sàrl, St-Sulpice, Switzerland

E-mail: vlad.hasmatuchi@hevs.ch

Abstract. Hydroelectric powerplants play a vital role in the electricity production mix, especially during the ongoing energy transition towards renewable sources. However, they face operational challenges due to harmful stress loading of various components. Ensuring safe operation remains essential for people's safety, electricity supply, and costs avoidance. The study focuses on penstocks and pipelines material damaging caused by fatigue, crack initiation and propagation. These critical components are often several decades old and expensive to refurbish or replace. Cycling loading, induced by pressure oscillations during start-stop or transient operations, accelerates material fatigue. Steel lining corrodes over time, and welds may contain original defects. To address this, a new testing facility that generates controlled cyclic pressure oscillations using the water hammer effect has been built. This specific closed-loop circuit allows accelerated fatigue testing of material probes, providing insights into crack initiation and propagation. The test rig operating principle is described while its 1D numerical model is introduced and validated with measurement data. The prediction of crack incipience and rupture of a tubular specimen with a pre-machined longitudinal weakening is in the end compared with the results of a fatigue test conducted on the test bench.

1. Introduction

Hydroelectric powerplants play a crucial role in the electricity production mix and particularly in the context of the actual massive integration of solar and wind energy production sources. In this scenario, they are often subject to a high operation flexibility and implicitly a harmful stress loading of all parts, including the penstocks. This study addresses the penstocks and pipelines material damaging caused by fatigue, crack initiation and propagation. The main source of fatigue consists of an accumulation of regular cyclic loading, created by pressure oscillations at each start-stop or during transient operations, coupled with isolated extreme load sequences induced by more rare events such as emergency shutdowns. Pipeline and penstocks are extremely critical regarding this type of damaging as they were often built several decades ago and are extremely expansive to refurbish or to replace. Furthermore, steel lining also suffers from corrosion and welds are prone to contain original defects such as porosities, lack of fusion and even cracks that can be growth under mechanical stresses. This may conduct to incidents or on the most catastrophic scenario to accidents (see the cases of Lapino [1] or Cleuson-Dixence [2]).

Beyond a regular pressure loading, occasional fast transient sequences may conduct to feared water hammer effects and either exceeding the maximum allowed overload or inducing water column separation. The possible impacts of water hammer on hydraulic power units are highlighted in a rich review in [3], whilst in [4] an extensive historical review on the water hammer with column separation from the discovery of the phenomenon in the late 19th century to the integration of standard models in nowadays commercial software is provided. In the case of an increase of operation flexibility of a powerplant, a prior study of possible premature fatigue of the penstock is mandatory. In [5], the possible penstock fatigue induced by a change of operating mode to perform secondary control of the grid was evaluated for a 69 MW pumped-storage powerplant. Then, in [6] the risk of penstock fatigue of a

Content from this work may be used under the terms of the Creative Commons Attribution 4.0 licence. Any further distribution of this work must maintain attribution to the author(s) and the title of the work, journal citation and DOI.

pumped-storage power plant induced by an operation with variable speed in pump mode at part load was evaluated and the maximum number of operating hours per year without generating penstock fatigue damages was quantified. In the end, a particular critical situation that may arise during the commissioning procedures, as treated in [7], is the so-called "Peak of Michaud" generated by an opening of the nozzles of a Pelton turbine followed by an immediate reclosing (for example due to an emergency shut down) which may lead to an excessive overpressure. The same level of importance as for the prior careful evaluation of transient impacts must be put on the continuous monitoring of pressure loading and in the ideal case on the real-time prediction of the remaining lifetime. In [8], the HydroClone® real-time simulation monitoring system deployed on 200 MW powerplant has been successfully used to quantify the accumulated penstock fatigue damage induced by past and future operations. The simulated predictions have been validated with on-site measurements of strain-gauges deployed on the penstock.

According to [9] and [10], classical machines for material fatigue testing may be classified in servo-hydraulic and in electrodynamic tables, adequate for testing of both plate and cylindrical specimens. In [11], the crack propagation for high-pressure gas pipeline walls with various defects has been experimentally assessed using mechanical circumferential loading of curved specimens, whilst in [12] tubular specimens have been stressed with 1 Hz cyclic internal pressure fluctuations generated by an oil pump coupled with a relief valve to evaluate the fatigue damage at welded tube joint.

Water hammer test rigs are often constituted by a pipe with a given length connected at one end to an upper reservoir and on the other to a valve with controlled fast closure/opening, able to generate one pressure wave at a time. The amplitude of generated water hammer is mainly dependent on the initial discharge and on the closing/opening time of the valve. In [13], a water hammer test rig with gravitational flow and continuous air entrainment has been used to validate a numerical model. Then, in [14] a water hammer open-loop test rig has been set up to experimentally investigate this phenomenon with cavity collapse under multiple interruptions. Finally, in [15] a specific test bench designed to reproduce the priming procedure including the main elements of a satellite propulsion system subject to fluid hammer with phase change occurrence induced by fast opening of a valve has been set up and equipped with a transparent module to visually characterise the hammer wave effects.

In the framework of this work, the water hammer effect is used for cyclic pressure loading of tubular probes to experimentally investigate the induced material fatigue, a set up considered more representative for fatigue damage in penstocks.

2. Theoretical principle of the fatigue experiments

2.1. Material fatigue of a tubular specimen

Fatigue refers to the progressive and localized structural damage that occurs when a material is subject to cyclic loading. For a tubular specimen, such as a penstock, the fatigue process can be particularly relevant due to the repeated internal pressures it experiences. The fatigue involves the initiation, propagation, and final fracture of cracks due to cyclic stresses induced by internal pressures.

During initiation, microcracks form at the surface or at stress concentrators, such as surface imperfections, inclusions, or grain boundaries. Then it propagates, meaning that these microcracks gradually grow with each loading cycle, expanding both laterally and in depth. Eventually, fracture occurs when the remaining cross-section of the material can no longer support the applied load.

- 2.1.1. Relationship between pressure and material stresses. As detailed in [16], in a tubular specimen, the internal pressure generates different types of nominal stresses:
 - Hoop Stress ($\sigma_h = p \cdot r/e$, with p the internal pressure, r the inner radius of the tube, and e the wall thickness): Also known as circumferential stress, it acts tangentially to the circumference of the tube.
 - Longitudinal Stress ($\sigma_l = \sigma_h/2$): Also named axial stress, it acts along the length of the tube, being usually lower than the hoop stress.
 - Radial Stress (σ_r): This stress acts radially inwards and is typically much smaller than hoop and longitudinal stresses in thin-walled tubes.

When periodic alternating pressure is applied, the tested specimen experiences cyclic stresses, with the maximum and minimum values proportional to the applied pressure fluctuations.

2.1.2. Link between stresses and Wöhler curve (S-N curve). Fatigue strength is defined as the stress level at which failure occurs after a specified number of cycles. It can be assessed by applying different levels of cyclic stress to individual test specimens whilst recording the number of cycles to failure. In the end, the so-called Wöhler curve, characteristic to each material, is obtained by a graphical representation of cyclic stress amplitude on the vertical axis (S) versus the number of cycles to failure on the horizontal axis (N). In addition, other important parameters must be considered, such as the range of stress ($\Delta \sigma$) experienced by the material, the stress amplitude ($\Delta \sigma/2$), the mean stress (σ_m) and the load ration (R), expressed as:

$$\Delta \sigma = \sigma_{max} - \sigma_{min}$$
; $\sigma_m = \frac{\sigma_{max} + \sigma_{min}}{2}$ and $R = \frac{\sigma_{min}}{\sigma_{max}}$ (1)

S-N curves are often generated for specific load ratios. Different load ratios shift the S-N curve up or down based on the nature of the cyclic loading. High stress amplitudes lead to a low number of cycles to failure, while low stress amplitudes can lead to a high number of cycles to failure, respectively shifting the S-N curve downward or upward. Higher mean stresses, like tensile stress, reduce fatigue life, while compressive mean stresses can enhance it. This can be faithfully represented by the Goodman line on a mean versus alternating stresses diagram, quantifying the interaction of those parameters on the fatigue life of a material. Theoretically, this curve represents the lifetime of the material, but experimentally, the stress can be increased locally to ensure that the experiment lasts a reasonable period. A controlled way of doing this is to design a notch on the sample or reduce its cross-section over a desired area. A theoretical, or geometric, stress-concentration factor ($K_t = \sigma_{max}/\sigma_0$ for normal stresses) is then used to relate the actual maximum stress at the discontinuity to the nominal stress.

2.2. Cyclic loading based on water hammer phenomenon

The well-known, generally undesired, water hammer phenomenon generating pressure surge in hydraulic systems is mainly governed by the closing time $t_{closure}$ of a downstream valve, the initial flow speed C_o , the distance L between the obstruction (valve) and the upstream reflection point (a severe enough section change) as well as the speed of sound a at which the wave will travel in the system. For a piping system, such as penstocks, according to [17], the speed of sound depends on the Young modulus of the liquid E_w (generally water), as well as on the pipe inner diameter D, wall thickness e, and Young modulus E_p , see Eq. (2). Even though for freshwater the speed of sound neighbours $1'480 \, m/s$, depending on the pipes properties as well as on the amount of gas contained in the water, in practice very low values (down to for example $50 \, m/s$) may be experienced.

$$a = \left(\rho \left(\frac{1}{E_w} + \frac{D}{e \cdot E_p}\right)\right)^{-1/2} [m/_S] \tag{2}$$

Then, the maximum overpressure amplitude may be estimated by two relationships specific to different distinct scenarios, on which the closure time of the downstream valve is either lower or greater than that necessary to the wave to travel go and back between the obstruction and the reflection points (equal to $2 \cdot L/a$):

$$\Delta p_{max} \cong \begin{cases} \rho \cdot a \cdot C_o [Pa], & \text{if } \frac{2 \cdot L}{a} \ge t_{closure} \\ \frac{\rho \cdot 2 \cdot L \cdot C_o}{t_{closure}} [Pa], & \text{if } \frac{2 \cdot L}{a} < t_{closure} \end{cases}$$
(3)

However, if for simple well-defined test cases all these parameters may be estimated analytically, for more complex systems composed of a chain of different elements between the obstruction and the reflection points (see the test case of penstocks), transient calculations that considers all these variables, coupled with experimental measurements, are often necessary.

For the present case, the benefit of water hammer phenomenon is used to generate cyclic pressure loading in a closed-loop test bench (see the schematic representation in Figure 1). Consecutive obstructions on the main flow, provided by a recirculation pump, are induced by a rotating ball-valve. The pressure waves thus generated, travel toward the system upstream up to the reflection point represented by the connection with an intermediate pressurised reservoir with free surface. On the way

back, these waves cross those generated by upcoming obstructions. At the mid-distance between the obstruction and the reflection points, a fatigue test section is installed. The adjustment of the rotational speed of the ball-valve allows us to join the forward and the backward waves at the test section which maximises the amplitude of the obtained pressure fluctuations.

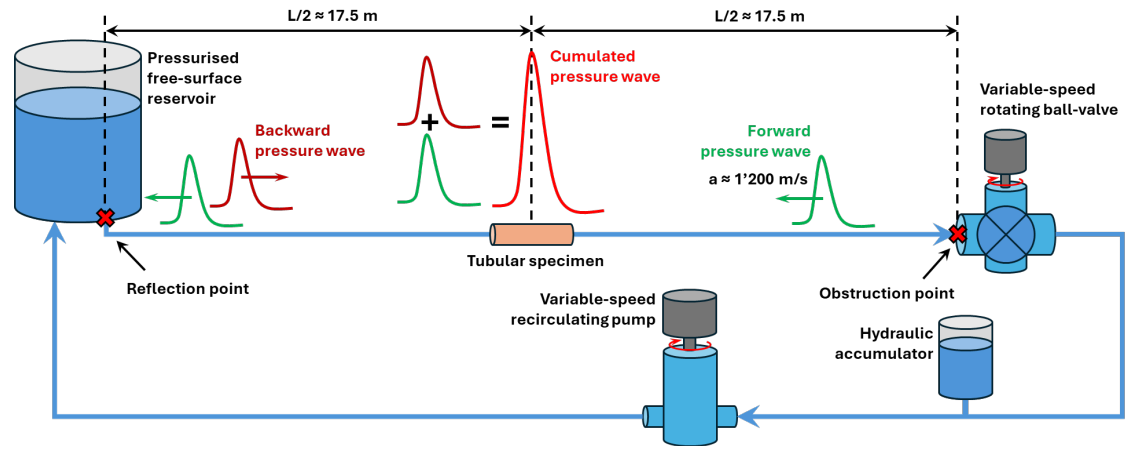


Figure 1. Schematic of a cyclic water hammer generator.

Basically, the rotating valve enables us to reach hydroacoustic resonance of the pipe between its two ends targeting the half wavelength natural mode shape of the pipe with pressure node at both ends and anti-node at the pipe middle, see Figure 2. Since the rotating valve is located at a discharge anti-node, it is capable to strongly excite the half wavelength mode shape of the pipe. This natural frequency can be estimated as $f = a/(2 \cdot L) Hz$. With the total pipe length of 35 m and a theoretical pipe wave speed of $1'200 \, m/s$ the natural frequency of the half wavelength mode is estimated to $17.15 \, Hz$, which is in good agreement with the experimental value found at $17.5 \, Hz$. The test rig was designed to reach hydroacoustic resonance of the pipe to obtain high pressure fluctuations amplitude rather than high excitation frequency of the tubular specimen. Since the rotating ball-valve does not correspond to an open-end boundary condition, the mode shape excited during the experiments on the HES-SO test rig does not feature perfect half wavelength value with pressure node at both ends but exhibits some pressure fluctuations amplitude in front of the rotating valve (see the results in chapter 4.2).

An asynchronous obstruction rate not only renders the system inefficient, but also induces undesired secondary pressure waves in the rest of the hydraulic circuit. The hydraulic accumulator installed at the recirculation pump upstream comes to damp these pressure fluctuations and the eventual harmonics of the phenomenon and thus to protect it. The amplitude of the generated pressure waves is controlled through the recirculation flow discharge by adjusting the rotational speed of the pump, whilst the average pressure on the test section is controlled by the pressure of the air in the upstream reservoir.

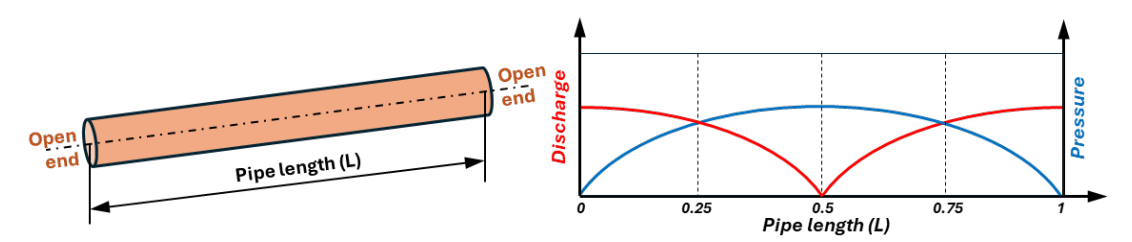


Figure 2. Theoretical pressure and discharge mode shape of a pipe with two open ends, [18].

3. Main characteristics of the test rig

3.1. The hydraulic circuit

A specific testing facility dedicated to the experimental study of material damaging induced by cyclic pressure oscillations has been built (see the preliminary set up [19]) and commissioned at the HES-SO VS in Sion, Switzerland, in 2023. The main components of this closed-loop hydraulic circuit are provided in Figure 3. The recirculating pump (1) with variable speed installed on the test rig can deliver

up to 15 m³/h and 16 bar. A rotating ball-valve (5), specially engineered for this purpose, similar with those introduced in [20] and [21], driven at variable speed, is used to induce about 17.5 pressure oscillations per second. The fast-cyclic obstruction of the main flow induced by the rotating valve conducts to a sinusoidal pressure oscillation at the test section (4), located at half distance between the rotating valve and the upstream reservoir, where the tubular testing probes are installed. Peak-to-peak pressure fluctuations of maximum 0 to 30 bar are obtained by a precise superposing of the traveling forward and backward pressure waves (dependent on the characteristic time and finally on the distance between the obstruction and reflection points, of about 35 m, as well as on the speed of sound) through the fine-tuning of the rotating valve speed. Both the mean pressure (through compressed air in the main upstream reservoir (3)) and the amplitude of pressure fluctuations (through the operating discharge, measured with the electromagnetic flowmeter (2)) are adjustable. The hydraulic accumulator (6) along with a check valve installed at the pump outlet are used to protect the latest by eventual secondary pressure waves. Finally, a counter-current axial mono-tubular heat exchanger, installed on the main loop of the test rig, is used to maintain the water temperature in the test bench constant during the fatigue experiments which may last from few minutes to several hours.

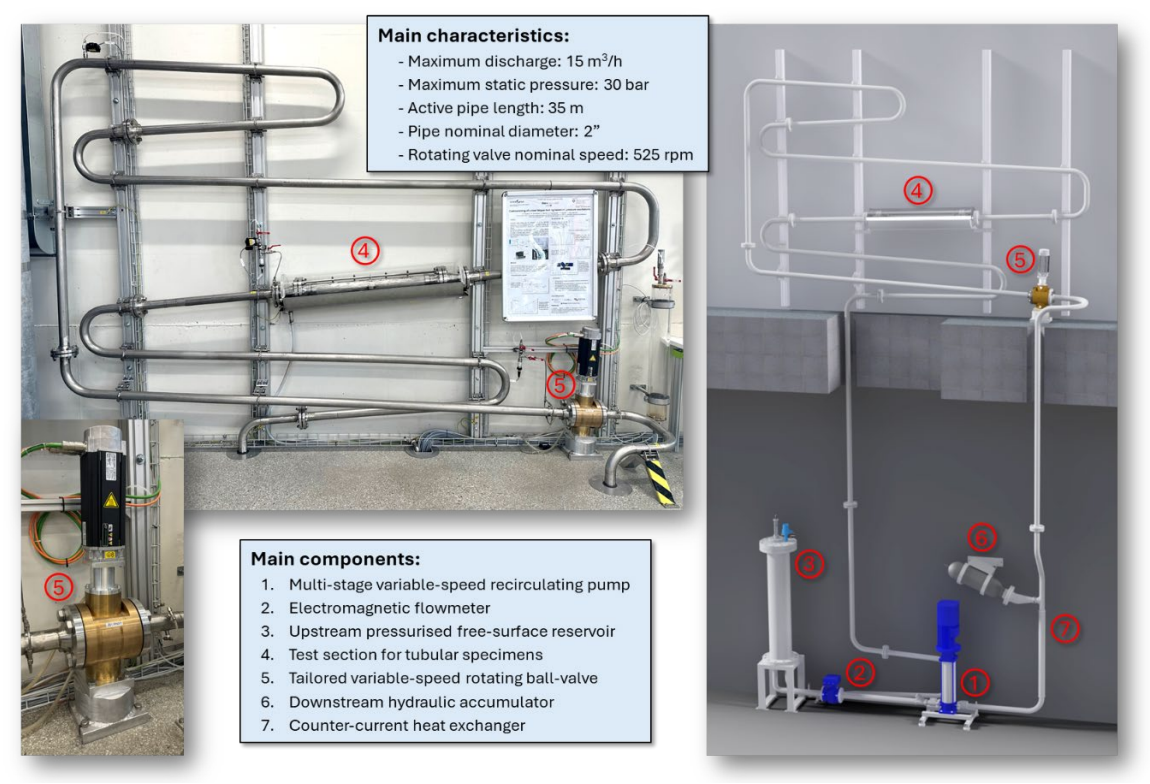


Figure 3. Main components and characteristics of the HES-SO VS water hammer fatigue test rig.

3.2. Instrumentation, control, and safety

An electromagnetic flow meter is used to measure the discharge, whilst several static pressure probes are installed mainly on the upstream pressurised reservoir, at the test section, at the inlet of the rotating ball-valve, as well as close to the hydraulic accumulator. The water level into the upstream reservoir is measured with the help of a capacitive level sensor. Two PT100 probes are used to survey the water temperature into the test rig and the heat exchanger. The rotational speed of the pump is determined with a photoelectric proximity sensor that provides one impulse per tour, whilst the rotational speed of the ball-valve is measured with an incremental encoder integrated in its servomotor.

The control of the test rig is ensured through a customised LabVIEW HMI deployed on a National Instruments cRIO 9035 controller able to autonomously handle in real-time all regulation and security functions. Several dedicated modules installed on the controller chassis are used to control all the elements of the test rig such as numerous solenoid valves or the recirculation pump and to get feedback

from various sensors and elements. The controller manages simultaneously the regulation of the main components (pump speed, valve speed, tank pressure, water temperature, etc.), the survey of leakage detectors and of the water level and pressure limits, and the continuous acquisition, display and recording of data provided by the different sensors. The rotational speed of the recirculation pump is controlled through a frequency converter integrated on its motor. The speed and/or the phase of the motor that entrains the ball-valve is controlled with the help of a Nidec M700 frequency converter either on permanent rotation or on phase change modes (for controlled one-shut open/close of the valve) respectively. The continuous synchronous acquisition of signals is performed at a rate of 1'000 Hz and recorded either as raw data (for dynamic measurements) or as statistical values (mean, amplitude and STD) from variable samples number. Generally, statistical values of all main process parameters are recorded during the whole fatigue test duration, whilst the raw data is only kept for several tens of seconds at different moments during the test.

4. Numerical modelisation of the test rig

4.1. Numerical 1D model

The SIMSEN® software developed by EPFL [18] allows 1D time-resolved simulation of main hydraulic components (pipes, valves, surge tanks and vessels, turbines and pumps) based on equivalent electrical scheme representation. The system of equations is defined by the Kirchoff laws and a Runge-Kutta 4th order procedure is employed to achieve the time integration of the full system, [22]. The capability and adequacy of this software to simulate transient scenarios from simple and very complex hydraulic schemes is largely proven through various test cases available in the literature.

4.1.1. Numerical layout. The numerical 1D model provided in Figure 4 considers the main components of the closed-loop circuit of the test rig including the variable-speed recirculation pump, the upstream pressurized reservoir, the variable-speed rotating valve, the hydraulic accumulator, and the connection pipes. For simulation initialization purposes, three valves and an upper and a lower reservoir have been additionally placed, being isolated during the transient simulation process. The main cross section changes on the pipes are also considered.

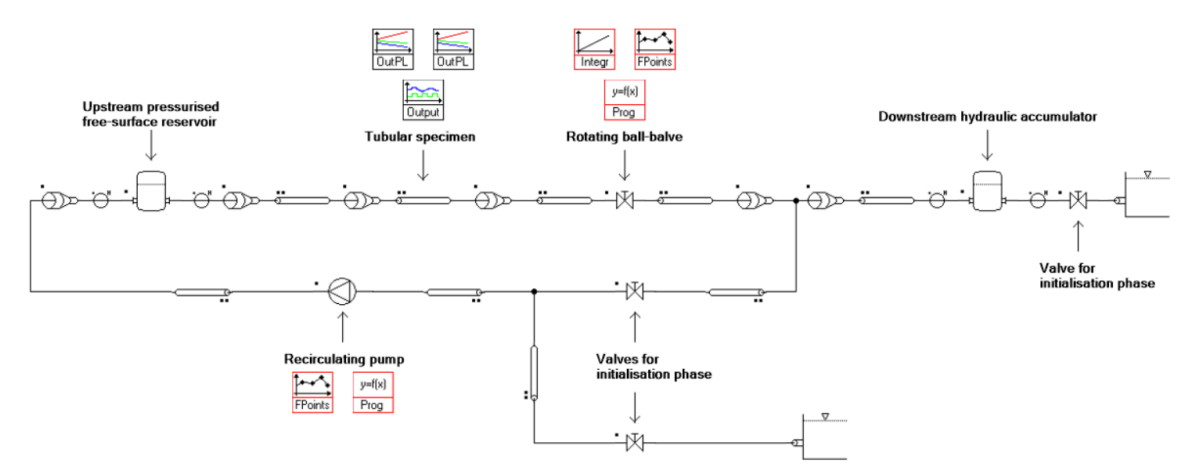


Figure 4. Numerical SIMSEN® 1D model of the test rig.

4.1.2. Numerical setup. During the first initialisation phase, the height of the upper and lower dams is set up in such way that the resulting static pressure in the upstream and downstream pressurised vessels reaches the desired water level and pressure. At this stage, the model considers an open-loop circuit with the help of the three indicated valves (the two placed close to the dams opened and the third one closed). The rotating ball-valve is set open and the pump in stand-by. At the second phase of the initialisation, the same three valves are set in opposite state, so the two dams are isolated, and the test bench loop is closed. Then, during the time-dependent simulation, the characteristics of the recirculation pump (discharge, pressure, and rotational speed) are used by the model to define its operating point depending on the imposed rotational speed-time scenario (with a given acceleration ramp) and on the pressure losses of the circuit. At the same time, a function is used to switch the rotating ball-valve on and off at

the same rate used on the test rig. With the imposed characteristics of the pipes located between the upstream tank and the rotating ball-valve (mainly the length, the inner diameter, and the head losses coefficient) the speed of sound is fine-tuned in such way that the forward and backward waves meet at the test section. The time-history of the discharge and the pressure for all sections of the circuit is the result of the simulation.

4.2. Numerical and experimental results

In the left side of Figure 5, the resulting time history of pressure fluctuations obtained at the test section and close to the ball-valve are compared to those measured on the test rig. One may state that both the rate, the amplitude and the mean values of the pressure fluctuations are fairly in good agreement between the simulation and the measurements. The average pressure value corresponds to the one set on the test rig with the help of pressurised air injected in the upstream reservoir. The pressure oscillation rate of 17.5 Hz corresponds to the one imposed on the test bench by the ball-valve rotational frequency (equal to half of the obtained oscillation, since the valve induces two obstructions per rotation). Finally, at the nominal rotational speed of the ball-valve, the amplitude of the pressure fluctuation is two times higher at the test section than that obtained close to the ball-valve. On the right side of Figure 5, the resulting simulated envelope of pressure and discharge fluctuations along the pipe clearly shows that the half mode shape of the pipe is excited, with the pressure anti-node located on the middle of the pipe where the mode tubular specimen is installed.

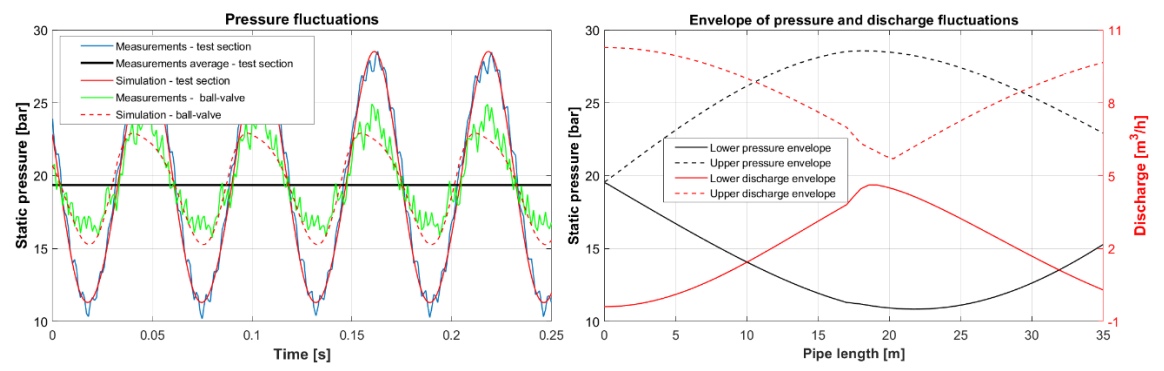


Figure 5. Time history of static pressure fluctuations at the test section and at the rotating valve (left) and resulting simulated envelopes of pressure and discharge fluctuations in the pipe (right).

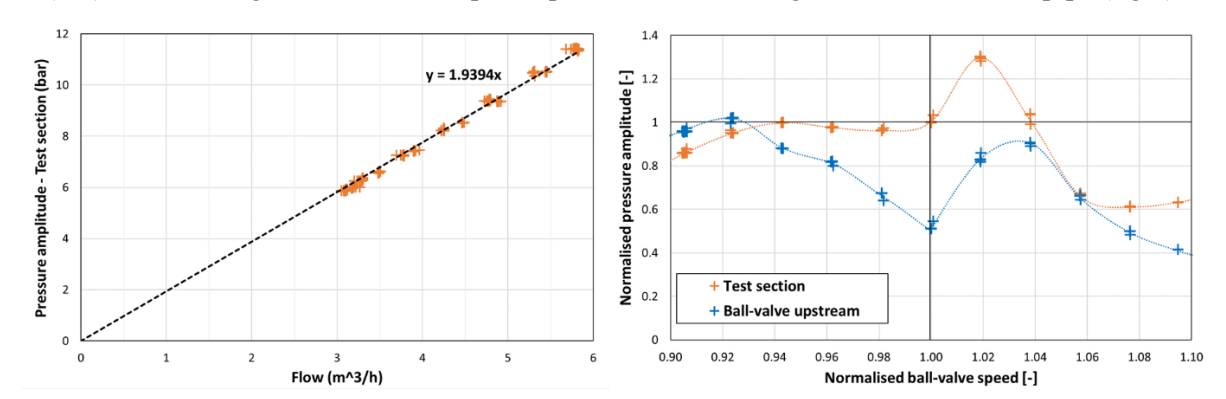


Figure 6. Resulting discharge-pressure amplitude relationship (left) and the influence of the rotational speed of the valve on the amplitude of pressure oscillations (right).

As explained in the subchapter 2.2, the fact that the rotating valve does not represent an open-end condition at the pipe downstream, the obtained amplitude of pressure fluctuations is not zero at the ball-valve. The obtained discharge node is located close to the middle of the pipe, whilst the anti-nodes are found at the pipe upstream and downstream ends. Then, in the left side of Figure 6 the resulting amplitude of pressure oscillations measured at the test section shows a linear variation with the discharge (in accordance with Eq. (3) that shows a linear relationship between the amplitude of a water hammer and the initial discharge). In the right plot, considering a fixed flowrate, the influence of the rotating

ball-valve speed variation on the resulting pressure amplitude at the test section and at the ball-valve is provided. The pressure amplitude is scaled with the value obtained at the test section for the nominal speed. The results show a ratio of two between the pressure amplitudes at the test section and at the ball-valve for the nominal speed, whilst it varies when changing the valve speed due to the phase shift of the traveling waves with all the undesired consequences such as high vibration of all the test bench sections, noise and large pressure fluctuations downstream the rotating valve.

5. Experimental crack of a tubular probe

5.1. Case study

A first fatigue test has been conducted on a tubular specimen made of AW-6060-T6 Aluminium extruded alloy, heat treated, quenched, and artificially aged, with the geometry provided in Figure 7. This material, instead of steel, has been chosen for these first tests for considerations of time-consuming, learning, machining efforts and availability of tubular probes for multiple testing.

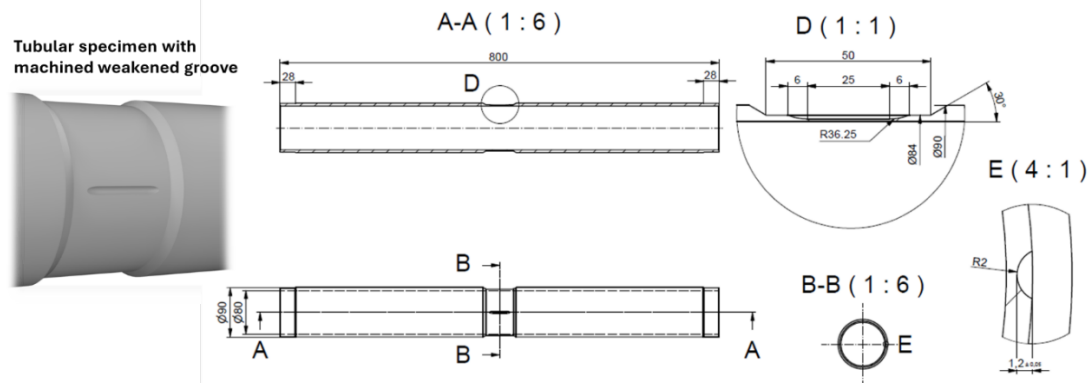


Figure 7. Geometry of the tested tubular specimens.

The present tubular specimen has a total length of 800 mm, an inner diameter of Ø80 mm and a wall thickness of 5 mm. The ends of the tube have been machined to fit the diameter and tolerances of the test section. One may note here that once installed, the tube is free of axial constraints (excepting the friction induced by the radial O-ring sealing). At the centre, the outer diameter of the tube has been machined on a section of 50 mm length to reduce the wall thickness to only 2 mm. Finally, a longitudinal groove has been additionally machined on one side of the tube to weaken even more the probe. For this first test, the remaining wall thickness at the bottom of the groove has been fixed to only 0.8 mm.

5.2. Theoretical crack prediction

To predict the cracking behaviour of the specimen, attempts have been made to estimate the stress concentration factor using analytical methods, such as Roark's or Peterson's equations. However, none of these truly represent the notched specimen and its mode of loading. Neither did the carried-out FEM analysis, since these predictions were not in line with the test results. In any case, the heavily notched specimen has been subject to cyclic loading and ended up with fatigue damage.

5.3. Experimental crack test results

As illustrated in Figure 8, the specimen underwent a total of $1.47 \cdot 10^5$ pressure loading cycles until a crack appeared (representing almost two and a half hours), and then it continued to propagate during $1.23 \cdot 10^4$ additional cycles. This clearly demonstrates fatigue work on the specimen and rules out any suspicious sudden damage. A slight reduction in the amplitude of pressure oscillations during this crack propagation phase, corresponding to the last period of operation on the graph, may be noticed. This is explained by the leakage of water through the crack, which relieved the internal pressure, but which remained important enough to propagate the crack along the groove in a leak-before-break configuration. In order to draw a Wöhler curve representative of the situation, it is needed to obtain a precise value of the stress concentration factor K_t to be able to exploit the following data: $\sigma_{max} = 25.2 \cdot K_t MPa$ and $\sigma_{min} = 9 \cdot K_t MPa$, giving $\Delta \sigma = 16.5 \cdot K_t MPa$; $\sigma_m = 17.25 \cdot K_t MPa$ and R = 0.35. Plotting the Wöhler curve will enable us to establish the Paris law to estimate the crack growth rate, and to deduce by integrating the law at the critical crack length a_C (when the stress intensity factor reaches

the material's fracture toughness), the number of cycles N_f to failure, and then approach the fatigue limit σ_D . Finally, the crack profile shows in Figure 9 an imperfect rectilinear crack, revealing a possible intergranular fracture. To confirm this hypothesis, SEM observations must be additionally carried out.

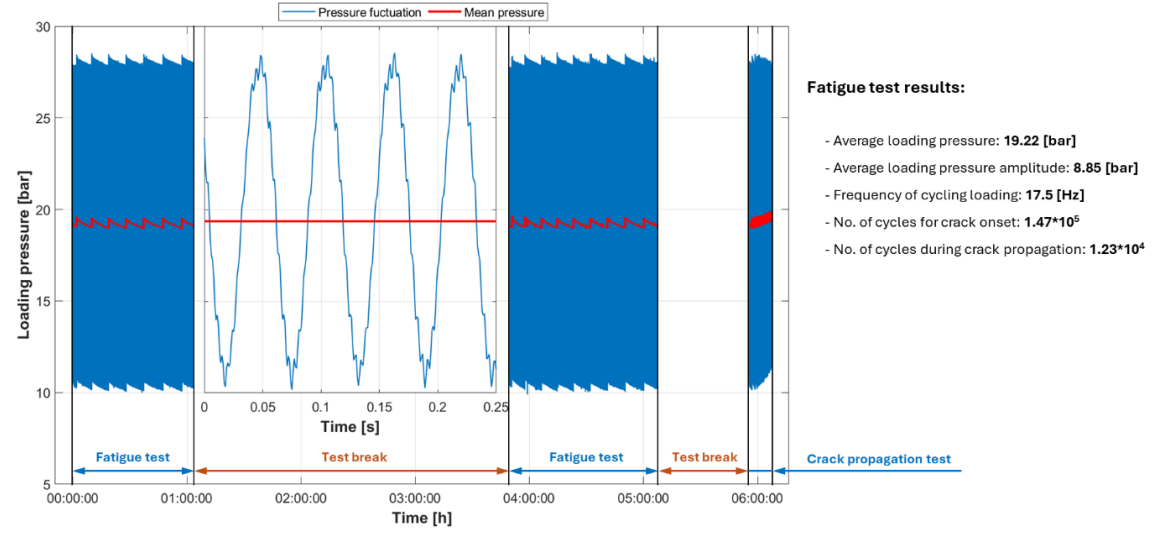


Figure 8. History of water hammer pressure induced oscillations and results of the fatigue test for a tubular specimen.

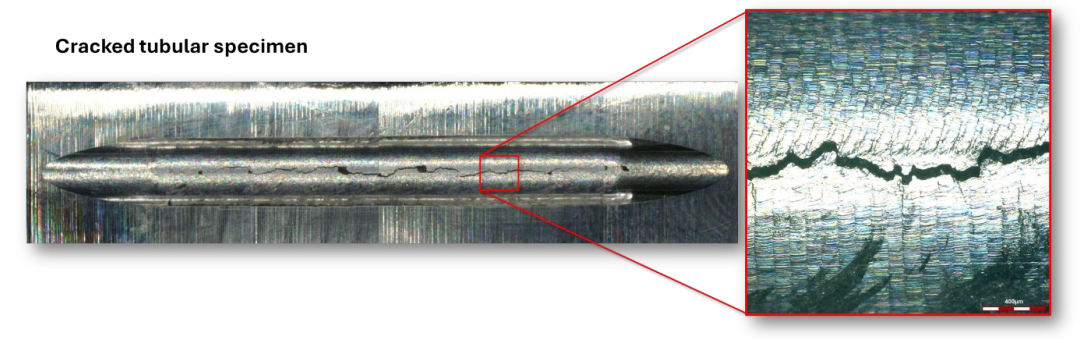


Figure 9. Photograph of the cracked tubular specimen.

6. Conclusions and perspectives

A new experimental facility dedicated to fatigue testing of metallic tubular specimens has been introduced. The test rig takes the benefit of the water hammer induced pipe resonance phenomenon to induce controlled cyclic pressure loading for accelerated material crack's onset and propagation. Its specific architecture allows generating pressure oscillations on the test section, placed at the middistance between a variable speed rotating ball-valve and an upstream pressurised reservoir with free surface, with a peak-to-peak amplitude from 0 to 30 bar at a rate of 17.5 Hz. Both the average static pressure and the amplitude of generated pressure fluctuations are adjustable. The results of the 1D SIMSEN numerical model of the test rig, in good agreement with the experimental measurements, show a sinusoidal pressure fluctuation at the test section with an amplitude two times larger than the one observed close to the rotating ball-valve at the nominal speed. In the end, the results of a first fatigue test conducted on tubular specimen made of an Aluminium AW-6060-T6 alloy have been provided along with the resulting accumulated number of stress cycles until the crack onset and forward towards the complete crack propagation. Further complete fatigue tests on specimens with different weakened wall thickness are planned to complete the data necessary to corroborate the obtained results with the material properties and the imposed stresses.

Acknowledgments

The present testing facility was realised with the financial support of the Institute of Systems Engineering, the Hydro Alps Lab of the HES-SO VS in Sion, Switzerland and the SCCER - Supply of

Electricity Swiss program, supported by the Innosuisse - Swiss Innovation Agency. The current fatigue tests are caried out within the WISE project, funded by the EU's Horizon 2023 research and innovation programme under grant agreement No. 101138718. The authors would like to address a special thanks to Anthony Gaspoz and the rest of the HES-SO VS staff involved in the development of this test bench.

References

- [1] Adamkowski A 2001 Case Study: Lapino Powerplant Penstock Failure *J. of Hydraulic Engineering* **127**(7), pp 547-555.
- [2] Chene O 2009 Welding Processes for the Cleuson Dixence Shaft *Proc. Conf. on High Strength Steels for Hydropower Plants*, Takasaki, Japan, Jul. 20-22.
- [3] Lupa S-I Gagnon M Muntean S & Abdul-Nour G 2022 The Impact of Water Hammer on Hydraulic Power Units *Energies* **15**(4), 1526.
- [4] Bergant A Simpson A R & Tijsseling A S 2006 Water hammer with column separation: A historical review *J. of Fluids and Structures* **22**, 135-171.
- [5] Nicolet C Berthod R Ruchonnet N & Avellan F 2010 Evaluation of Possible Penstock Fatigue Resulting from Secondary Control for the Grid, *Hydro 2010*, Lisbon, Portugal, Sep. 27-29.
- [6] Martínez-Lucas G Perez-Díaz J Chazarra M Sarasúa J Cavazzini G Pavesi G & Ardizzon G 2019 Risk of penstock fatigue in pumped-storage power plants operating with variable speed in pumping mode *Renewable Energy* **133**, pp 636-646.
- [7] Bissel C Vullioud G Weiss E Heimann A Chene O Dayer J-D & Nicolet 2011 Recommissioning of the Bieudron powerplant *The Int. J. on Hydropower & Dams* **18**(3), pp 82-85.
- [8] Dreyer M Nicolet C Gaspoz A Biner D Rey-Mermet S Saillen C & Boulicaut B 2019 Digital clone for penstock fatigue monitoring *IOP Conf. Series: Earth and Env. Sc.* **405**, 012013.
- [9] Marques J Benasciutti D Niesłony A & Slavic J 2021 An Overview of Fatigue Testing Systems for Metals under Uniaxial and Multiaxial Random Loadings *Metals* 11(3), 447.
- [10] Shawki G S A 1990 A Review of Fatigue Testing Machines Engineering J. of Qatar Univ. 3.
- [11] Gajdoš L & Šperl M 2012 Evaluating the Integrity of Pressure Pipelines by Fracture Mechanics, In book: Applied Fracture Mechanics, Belov A Ed., *IntechOpen: Rijeka*, Chapter 10.
- [12] Chen X & Zhao S-M 2005 Evaluation of fatigue damage at welded tube joint under cyclic pressure using surface hardness measurement *Engineering Failure Analysis* **12**, 616-622.
- [13] Zhang B Wan W & Shi M 2018 Experimental and Numerical Simulation of Water Hammer in Gravitational Pipe Flow with Continuous Air Entrainment *Water* 10(7), 928.
- [14] Zhao L Yang Y Wang T Han W Wu R Wang P Wang Q & Zhou L 2020 An Experimental Study on the Water Hammer with Cavity Collapse under Multiple Interruptions *Water* 12(9), 2566.
- [15] Lema M Peña F L Buchlin J-M Rambaud P & Steelant J 2016 Analysis of fluid hammer occurrence with phase change and column separation due to fast valve opening by means of flow visualization *Experimental Thermal and Fluid Science* 79, pp 143-153.
- [16] Roylance D 1996 Mechanics of materials John Wiley & Sons New York, USA
- [17] Allievi L 1925 Theory of water-hammer English translation by E. E. Halmos *Typography R. Garroni* Rome, Italy.
- [18] Nicolet C 2007 Hydroacoustic modelling and numerical simulation of unsteady operation of hydroelectric systems *EPFL Thesis No 3751*.
- [19] Gaspoz A Gonçalves N Barras L Hasmatuchi V Nicolet C and Rey-Mermet S 2019 Commissioning of a new fatigue test rig based on pressure oscillations Poster in *SCCER-SoE Annual Conf. 2019*, Lausanne, Switzerland, September 3-4.
- [20] Blommaert G 2000 Etude du comportement Dynamique des turbines Francis: Contrôle actif de leur stabilité de fonctionnement *EPFL Thesis No. 2222*.
- [21] Landry C 2015 Hydroacoustic Modeling of a Cavitation Vortex Rope for a Francis Turbine *EPFL Thesis No 6547*.
- [22] Nicolet C Kaelbel T Alligné S Ruchonnet N Allenbach P Bergant A & Avellan F 2011 Simulation of Water Hammer Induced Column Separation through Electrical Analogy 4th Int. Meeting on Cavitation and Dynamic Problems in Hydraulic Machinery and Systems, Belgrade, Serbia.